Composition, structure, and electrical properties of $Bi_2Sr_2Ca_{1-y}Y_yCu_2O_8$: A single-crystal study

C. Kendziora, L. Forro,* D. Mandrus, J. Hartge, P. Stephens, and L. Mihaly
Department of Physics, State University of New York, Stony Brook, Stony Brook, New York 11794

R. Reeder and D. Moecher†
Mineral Physics Institute and Department of Earth and Space Sciences, State University of New York, Stony Brook, Stony Brook, New York 11794

M. Rivers and S. Sutton
National Synchrotron Light Source, Brookhaven National Laboratory, Upton, New York 11793
(Received 16 December 1991)

A systematic study of yttrium substitution for calcium in the high-temperature superconductor $Bi_2Sr_2CaCu_2O_8$ has been performed. Single crystals were grown, cleaved, and characterized with use of x-ray fluorescence, electron microprobe, and electron- and x-ray-diffraction techniques. The dc resistivity, diamagnetic shielding, and Hall coefficient of the samples were also measured as functions of the temperature from 4 to 300 K for different dopant concentrations. We conclude that our systematic substitution in the family $Bi_2Sr_2Ca_{1-y}Y_yCu_2O_8$ gives an insight into this high-temperature superconducting material as well as into weak localization and metal-insulator transitions.

INTRODUCTION

In the study of the superconducting and normal-state properties of the high-T_c cuprates, it is often of interest to create samples with a reduced transition temperature. Our principal motivation for the present study is to gather information about superconductivity by destroying it in various ways and studying the trends in the characteristic parameters of the system.

It is well established[1-9] that the transition temperature in the $Bi_2Sr_2CaCu_2O_8$ system can be adjusted by replacing Ca with Y. One would expect that yttrium, having a larger valence than calcium, would act as a dopant and smoothly decrease the conduction-electron density, while retaining the crystalline structure.

Tamegai *et al.*[2] were among the first to study the diffraction pattern and lattice parameters as well as the resistivity, Hall effect, and susceptibility of these compounds. Maeda and co-workers[3] measured the change in lattice constants, resistivity, susceptibility, Hall effect, and optical reflection. Ando *et al.*[6] measured these same properties excluding reflection and also measured the Meissner fraction. Fukushima *et al.*[5] measured diffraction, the *c* lattice parameter, resistivity, and magnetization. Groen, DeLeeuw, and Feiner[8] measured lattice constants, oxygen concentration, and resistance. Much of this work seems to have been motivated by the early efforts of Manthiriam and Goodenough,[7] who measured changes in resistance and lattice constants with yttrium substitution, as well as by the efforts of Yoshizaki *et al.*[4] who measured resistivity and susceptibility on yttrium-doped samples.

All of these studies, however, were performed on polycrystalline or ceramic samples. In the time elapsed since these experiments were completed, more groups have begun to concentrate on single-crystal samples, especially for doping studies. Mitzi and collaborators[1] have conducted the primary single-crystal yttrium-doping study, measuring lattice parameters, magnetization, susceptibility, and Hall effect. They also studied the composition of the crystals and were able to illustrate the inhomogeneous, polyphasic nature of grown crystals.

In this paper, we discuss the preparation and characterization of $Bi_2Sr_2Ca_{1-y}Y_yCu_2O_8$ single-crystal samples used in both infrared transmission[10,11] and tunneling[12] studies. Furthermore, we present the electrical transport properties and offer an analysis of the trends observed in the data.

PREPARATION

The crystals were grown from a powder charge comprised of Bi_2O_3, $SrCo_3$, $CaCO_3$, Y_2O_3, and CuO. The amount of Y_2O_3 was systematically varied in order to induce changes in the structural and electronic transport properties of the solid. The starting composition was stoichiometric [Bi]:[Sr]:([Ca]+[Y]):[Cu]=2:2:1:2; the relative amount of [Y]:[Ca] ranged from 0:1 to 1:0. (In this paper the symbol [ ] will be used to indicate the amount of the corresponding element.) Additionally, an extra 20–50 % of CuO was often, but not always, used as a flux to facilitate large crystal growth. We observed that the excess CuO flux aids the crystal growth of the more heavily doped samples, while it does not change the properties of the samples themselves in any apparent way other than crystal size.

The general routine was as follows: once measured and manually mixed, the powder charge (typically 200–300 g total mass) was put into a high-purity alumina crucible. It was then placed in the furnace and heated in about 4 h

to 1020 °C. The charge was maintained at this temperature until all of the powders had melted, a period of roughly 6 h. The cool down did not begin until a visual inspection of the crucible (through a hole in the top of the furnace) revealed a totally homogeneous (devoid of visible flakes) and slightly viscous fluid. The mixture was then stirred with an alumina rod to insure the homogeneity of the melt.

The cooldown began at 1020 °C and continued to 840 °C at a rate of 1.6°/h, a process which takes just over 4 days. From 840 °C, the crucible was cooled much more quickly (approximately 10°/h) down to room temperature. The solid-liquid phase transition was at approximately 900 °C for the undoped preparation. For a few batches we performed a crude DTA (differential thermal analysis) with a differential thermocouple attached to the crucible and to a hot reference point inside the furnace. The transition appeared fairly broad and it may depend on the Y concentration—hence, the wide, 180 °C range for the slow cooldown. Mitzi *et al.*[1] emphasized the influence of the temperature gradient on the crystal growth direction. In our furnace, the temperature gradient was a vertical one since we observed and stirred the samples through a hole in the top (center) of the furnace and the heated panels are below the crucible.

Once cool, the crucible was cracked open to reveal micalike flakes with shiny crystal faces. Crystals with surface areas as large as 1 cm^2 have been grown in the pure and slightly yttrium-doped samples (up to 10% nominal yttrium content). For larger yttrium concentrations the crystal size decreased rapidly, although it was possible to get single crystals with $y=1.0$ which had dimensions of approximately 1 mm$\times$1 mm. For this study, samples with nominal yttrium concentrations of $y=0$, 0.03, 0.06, 0.075, 0.09, 0.10, 0.12, 0.2, 0.5, and 1.0 (fully yttrium doped) were grown, prepared, and analyzed. The tendency of these crystals to cleave perpendicular to the c axis was exploited in a manner discussed elsewhere[13] to prepare thin, high-quality single crystals throughout the doping study.

The crystal growth was performed in air. It is well documented that annealing or "heat treatment" of $Bi_2Sr_2CaCu_2O_8$ samples has led to differences in T_c.[1,8,14,15] Our crystals have routinely shown superconducting transitions around 75 K (zero resistance) as grown. After heating the cleaved crystals in air to $\simeq$600 °C for as little as a minute, the T_c rises to typical values of 85–90 K. Conversely, heat treatment in He, vacuum, or any low oxygen pressure reduces the critical temperature. Under a variety of low oxygen pressures, annealing temperatures, and time spans we failed to see any increase in superconducting transition temperature. These observations suggest that the crystals are oxygen deficient when grown and that the critical temperature is increased by the oxygen uptake for oxygen pressures up to a few atmospheres (the largest tried).

Concerning this feature, the published data is contradictory: Mitzi *et al.*[1] observed improvement in T_c with heat treatment in low oxygen pressure, while Crommi *et al.*[15] agree with our findings. The oxygen deficiency, and the exact composition of other elements in the sample, may well depend on apparently subtle details of the preparation conditions, such as the heat distribution inside the furnace (it might be very important if the top or the bottom of the sample freezes first). We did not explore all these factors, and we did not have an independent control over all, potentially important, circumstances. A great effort was made, however, to ensure that the conditions were reproduced as closely as possible between subsequent preparations.

COMPOSITION

The composition of the melt-grown crystals is open to discussion, since typically there were large amounts of secondary material left in the crucible. Therefore, it was essential to perform composition analysis on the crystals. We selected two different methods: x-ray fluorescence, sensitive to (Y, Cu, Sr, Bi) and electron microprobe, sensitive to (Ca, Y, Cu, Bi, Sr). When the same element was analyzed with both methods, the results of the two methods generally agreed. We observed significant differences between the "nominal" and "actual" compositions, especially with respect to the amount of yttrium present in a given crystal.

The stoichiometric coefficients of the samples was studied with wavelength dispersive spectrometry on the Cameca CAMEBAX electron microprobe at SUNY Stony Brook. Absolute measurements of the elemental concentrations was achieved by comparing peak intensities of the unknown with those from well-characterized standards of known composition. Corrections were made for the matrix effects of atomic number, absorption, and fluorescence by other elements in the sample and in the standard, by using Cameca PAP, a ϕ-$\rho(z)$ correction scheme. All elements, with the exception of oxygen, were measured this way. For oxygen, the resolution of the instrument was not high enough to reach other than trivial conclusions.

In the electron microprobe we first looked for composition differences between the 2:2:1:2 crystals and the surrounding material. Such differences were visible in backscattered electron images, since the displayed gray scale is based on average atomic weight; the heavier phases appear brighter. For this we prepared samples by sanding and polishing a large amount of the solid with random crystallographic orientation. In such cases we observed the presence of several phases in addition to the 2:2:1:2 crystals. In particular, a bulk sample of undoped 2:2:1:2 showed small inclusions of copper (or copper oxide—we were not sensitive to oxygen), presumably from the flux. Also, an intermediately doped sample, nominally $y=0.12$, showed that there were some areas on the periphery which contained no yttrium at all. Similarly, a bulk sample of $y=1.0$ contained extraneous bismuth-free and copper-free phases as well as pure yttrium inclusions.

After this preliminary investigation, we performed similar measurements on thinly cleaved single crystals. In such samples (typical dimensions 1.0 mm$\times$1.0 mm$\times$1.0 μm) we saw no inclusions of different composi-

tion on the length scale of 1 μm or larger (smaller inclusions can not be resolved by the probe). However, for larger and thicker crystals, inclusions are likely to occur. Based on this observation we emphasize the importance of using thin single crystals in the study of the physical properties.

The composition analysis was performed on different crystals from the same batch, as well as on several spots in the same crystal. Apparently, the yttrium content varied even within a single batch. Variations within the same single crystal were much smaller, but further studies will be necessary to establish the length scale and the degree of uniformity.

Table I contains the measured concentrations for several members of the study, with the sum of the cations per formula unit fixed to seven for simplicity. The data represent the average figures for 10–30 different crystals of each nominal concentration.

The x-ray fluorescence studies were performed at The National Synchrotron Light Source at Brookhaven National Laboratory using the x-ray fluorescence beam line X-26A. Several crystals of each nominal yttrium concentration were mounted on copper grids and glass slides. The copper grids were washer-shaped with an inner diameter of 0.6 mm. The samples (most of which were transparently thin) were attached to the grid with a tiny drop of silver contact paste. Those samples mounted on slides were generally thicker, and were glued down (on the underside only) with nail polish. Calibration samples (pelletized powders of known composition and density) were also measured. The synchrotron (broadband) x-ray beam was incident on the samples with a spot size of approximately 10×10 μm. The fluoresced x rays were detected with a Si(Li) detector mounted 5 cm from the sample at 90° from the incident beam.

The Bi $L\alpha$, Bi $L\beta_1$, Bi $L\beta_2$, Sr $K\alpha$, Ca $K\alpha$, Cu $K\alpha$, and Y $K\alpha$ peaks were fit with Gaussian functions and the area above the background was calculated. The results were evaluated by comparing the intensities with the calculated intensities obtained from computer simulation.[16] Due to the energy dependence of the x-ray absorption, the sample thickness plays an important role in the evaluation of the data. Since the samples did not all have the same thickness and this dimension was not always known, certain peak intensities (because of their sensitive dependence on thickness) proved more difficult to measure. Because of the number of experimental parameters being varied from sample to sample, only the *ratios* of different peak counts are presented here. For reference we selected strontium since its atomic number (and therefore $K\alpha$ x-ray energy) was closest to yttrium, the compositional variable.

For the purposes of this study, the primary consideration was the yttrium content of the actual single crystals obtained from large preparations. The proximity of the yttrium line to the strontium (both $K\alpha$), as well as the thickness independence of the ratio between them, allows for quite accurate determination of the Y content, assuming that [Sr] does not change. Figure 1 displays the *measured* yttrium content versus *nominal* Y content for 31 independently measured samples. It must be stressed that it is the ratio of 2[Y]/[Sr] that is plotted. However, due to the invariance of the Sr composition with a change in the yttrium content and the thickness, the variation in this ratio can be fairly safely thought of as resulting solely from a real change in yttrium concentration. For comparison, we have also plotted the results of the electron microprobe study, taken from Table I.

Several aspects of the data represented in Fig. 1 warrant discussion. First, there is a preferential introduction of Y into the single crystals as they grow, indicated by the steep slope in the figure for nominal concentrations of less than 0.2. This is in good agreement with Mitzi's results.[1] Only a fraction of the initial powder charge grows in crystals which, by virtue of their size, are useful for experiments, hence, it is possible to find that some crystals contain 40% Y when the starting composition was only 10% Y.

It is of interest to note that, according to the x-ray fluorescence measurements, the composition saturates at about [Y]=0.8, distinctly different from the stoichiometric 2:2:1:2 expectation. Similar conclusions can be drawn from the electron microprobe study, and similar observations were made by other groups as well.[17–20]

Finally, the scattering of points for each nominal composition reflects the inhomogeneity between samples as they grow in the crucible. Indeed, there seems to be some correlation of T_c with the vertical origin of a given crystal within the crucible: the lower in the crucible, the higher T_c. This may be due to the fact that the crystal grows downward, preferentially incorporating Y, leaving less Y in the fluid for crystals at the bottom.

Bismuth concentration was measured by using the sum of the counts under the three bismuth lines (all L lines). Although individually thickness dependent, the sum of

TABLE I. The results of electron microprobe analysis. Starting powder charges correspond to $Bi_2Sr_2Ca_{1-y}Y_yCu_2O_8$ with yttrium contents as given in the "nominal" column. Error bars represent approximately one standard deviation of scatter in the data.

Nominal	Bismuth	Strontium	Calcium	Yttrium	Copper	Ca+Y
Y=0	2.14±0.04	1.93±0.05	0.92±0.03	0	2.02±0.04	0.92±0.03
Y=0.09	2.03	1.87	0.79	0.30±0.07	2.00	1.09±0.10
Y=0.12	2.01	1.86	0.65	0.44±0.05	2.05	1.09±0.08
Y=0.20	2.04	2.05	0.41	0.55±0.03	1.95	0.96±0.05
Y=0.50	1.91	1.95	0.53	0.64±0.02	1.98	1.17±0.05
Y=1.0	2.02	2.10	0	0.86±0.02	2.00	0.86±0.02

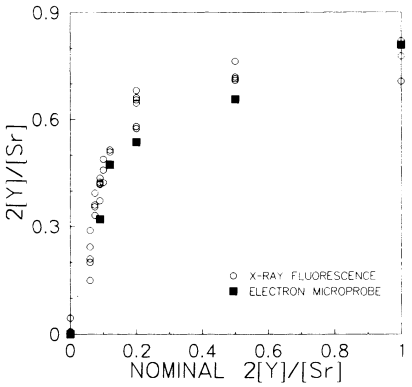

FIG. 1. The measured ratio of 2[Y]/[Sr] for single crystals is given as a function of nominal 2[Y]/[Sr] composition. Both x-ray fluorescence and electron microprobe data are shown. Yttrium is preferentially incorporated into those samples with lower concentrations and saturates at a value of [Y]=0.8.

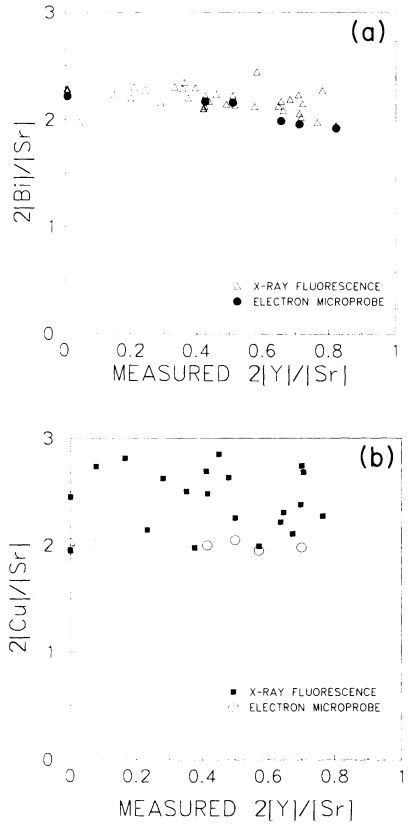

FIG. 2. The ratios of (a) [Bi]/[Sr] and (b) [Cu]/[Sr] for single crystals are plotted as functions of measured 2[Y]/[Sr] yttrium concentration (from x-ray fluorescence). Both x-ray fluorescence and electron microprobe results are shown. Bismuth and copper each appear to have larger concentrations than strontium in the fluorescence data, but only bismuth does so in the electron microprobe data. In general, the concentrations of these elements is independent of yttrium concentration.

the three lines turns out to be constant (to within a single percent) in the range of thicknesses between 0.1 and 10 μm. The concentration of bismuth in the single crystals was found to be about 5–10% higher than for Sr, in accordance with the electron microprobe results (Table I). The bismuth/strontium ratio is plotted in Fig. 2(a).

Figure 2(b) depicts the 2[Cu]/[Sr] ratio as a function of the measured Y-doping content. Since the copper sample holders would interfere with this measurement, only the 21 samples mounted on glass slides have been included. The sustained deviation of the ratio from the expected value [Cu]/[Sr]=1 has been seen elsewhere.[1,3,6,7,18–20] We argue that the x-ray fluorescence is a less reliable method for determining [Cu]/[Sr], since the technique relies on two lines (Cu $K\alpha$ and Sr $K\alpha$), which have very different thickness dependences due to x-ray attenuation in the sample. Although we made efforts to correct for these effects, such attenuation leads to a significant scatter in the data (as seen in the figure), and it may easily cause a systematic error of 10%.

In summary, for the Y end member, the x-ray fluorescence gives a composition of $Bi_\alpha Sr_\beta Y_\gamma Cu_\delta O_8$, where α=[Bi]=2.2±0.1, β=[Sr]=2 (fixed), γ=[Y]=0.8 ±0.05, and δ=[Cu]=2.2±0.2. The exact amount of oxygen was not determined in our study. If, instead of fixing strontium to 2, we fix the sum of the four cations to seven, we get α=2.12, β=1.94, γ=0.80, and δ=2.12. The [Bi]/[Sr] and the [Cu]/[Sr] ratios proved to be independent of the Y content. There is a good agreement between the x-ray fluorescence and electron microprobe results. In particular, the composition of the samples deviates from the "ideal" [Bi]:[Sr]:([Ca]+[Y]):[Cu] =2:2:1:2 in that there is an excess amount of Bi and Cu with a significant deficiency of Y and Ca.

STRUCTURE

The structure of the samples was studied by x-ray and electron diffraction. The x-ray study concentrated on the variations in the c lattice parameter of the crystals, while the electron diffraction produced diffractograms in the a^*-b^* plane. Because the individual samples used in these experiments were not measured for composition, all yttrium dopings listed are nominal. For actual compositions, the reader is referred to Table I.

As noted elsewhere,[1–9,21] substituting Y for Ca in 2:2:1:2 preserves the basic crystalline structure while decreasing the c-axis parameter and increasing both the a- and b-axis parameters. We have measured the c-axis modulation with Y concentration using a four-circle diffractometer and cleaved crystals. The x rays used were from the $K\alpha$ line (8.847 Å^{-1}) of a rotating Molybdenum anode.

Figure 3 shows the observed variation of the c-axis parameter for thin crystals with increases in yttrium content. Data points were arrived at from a Gaussian fit to the peak, with a least-squares value for the center and uncertainty therein. Typically, the reflections used were (0,0,8), (0,0,10), and (0,0,12) with the uncertainties in peak centers corresponding to 0.03 Å for (0,0,8) and 0.02 Å for (0,0,12) measurements. These uncertainties are

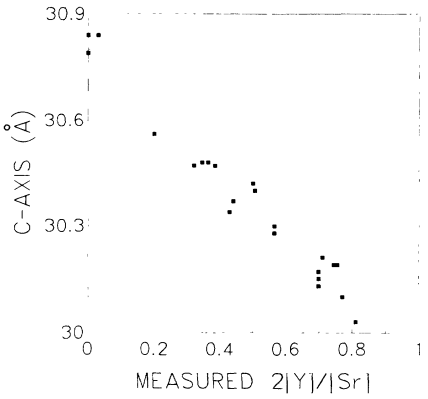

FIG. 3. The crystallographic c axis is plotted as a function of measured yttrium content 2[Y]/[Sr] (from x-ray fluorescence). The data strongly suggests a linear dependence of the c axis on Y doping. This is presumably due to the fact that yttrium atoms take up less space than the calcium atoms they are expected to replace.

roughly the scale of the data points themselves in Fig. 3. No attempts were made to increase the resolution. Working with thin single crystals is more difficult than with bulk samples, since the thinner ones bend, yielding a considerable mosaic and restricting the portion of the sample that satisfies the Bragg condition at any one orientation. As a consequence of this, all of the c-axis peaks were resolution limited (a full width of 0.1°, or $\simeq 0.1$ Å, in these terms) and no information could be garnered about the long-range order of the crystals.

It is interesting to note that, had the assumption been made that the c axis changed linearly with Y content, some of the same conclusions drawn from the composition analysis could have been made on the basis of these experiments alone. Specifically, these are the observations regarding the preferential introduction of Y into the Ca sites and the crystal-to-crystal inhomogeneity within the same crucible.

Due to the relatively low resolution of the x-ray measurement, the a and b lattice constants were both measured to be 5.40 ± 0.02 Å for the calcium end member. Although the orthorhombic structure is not apparent in the lattice spacing, it can be easily observed in the superlattice peak characteristic of modulation in the b direction.[1-3,8,21-24] The location of this peak at (0,2.213,0) is in good agreement with the generally accepted value of $4.7b$ for the superlattice modulation period. No attempt was made with x rays to observe the small changes in a and b with yttrium-dopant concentration.

The structural effects of doping on a, b, and the superlattice are most readily evident using a transmission electron-diffraction technique.[21-25] The photographs generated with this apparatus, wherein a 200-keV beam of electrons impinges upon a thin sample cleaved perpendicular to the c axis, map the a^* and b^* plane. Figures 4(a)–4(d) show the effects of increased Y content on both a and b. Naturally, the tiny changes in a and b themselves are difficult to discern on film. However, the broadening (smearing) of the peaks indicates a decrease in long-range order for a^*, b^*, and the superlattice—a fact which, if inherent, may explain the tendency for the heavily doped samples to grow smaller crystals.

Selected-area electron-diffraction (SAED) patterns were recorded using a JEOL 200CX transmission electron microscope operating at 200 keV. Cleaved thin flakes (typically 100–250 nm thick) of nominal composition [Y]=0.0, 0.075, 0.09, 0.12, 0.2, 0.5, and 1.0 were mounted on copper support grids with silver contact paint. SAED observations were limited to the [001] zone axis owing to the method of sample preparation. The fundamental 5.4×5.4 Å pseudotetragonal cell was observed for all compositions. Furthermore, the characteristic incommensurate modulation indicated by satellite reflections along b^* was present in all samples [Figs. 4(a)–4(d)]. Although not the focus of the present electron-diffraction work, the modulation wavelength was observed to decrease with increasing nominal Y content from approximately $4.7b$ in the Y-free material to 4.05–$4.1b$ in the pure Y compound. These results are in good agreement with those published in Refs. 2, 22, 21, 23, and 24. No evidence is found for twinning by rotation around the c axis. This is in contrast to the $YBa_2Cu_3O_7$ material, where this type of twinning is common.[26]

Satellites indicating an apparent secondary modulation

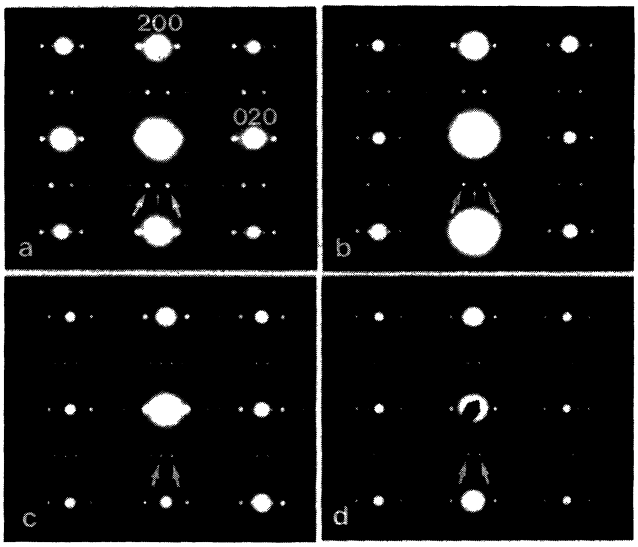

FIG. 4. [001] zone-axis selected-area electron-diffraction patterns of $Bi_2Sr_2Ca_{1-y}Y_yCu_2O_8$ thin specimens: (a) $y=0$, (b) $y=0.12$ nominal, (c) $y=0.2$ nominal, and (d) $y=1.0$ nominal. An incommensurate modulation occurs along the b^* direction, as indicated by the satellite reflections around, for example, 200 and 020. In (a) and (b), the corresponding first-order satellite reflections are indicated by arrows around the weak (and forbidden) $\bar{1}00$ spot (small arrow). In (c) and (d), first-order satellite reflections (arrows) are seen to have a separation half that in (a) and (b), and correspond to an apparent secondary modulation. In addition, the forbidden $\bar{1}00$ spot is absent in (c) and (d). In (c), diffuse streaking is observed between first- and second-order satellite reflections

were observed in samples with nominal Y contents of $y=0.2$ and 1.0 and possibly for $y=0.5$ (discussed below). These satellites were present only in rows along the b^* direction, where positions have $h+k=$odd, and are seen in Figs. 4(c) and 4(d) around the position of $\bar{1}00$ (a forbidden reflection). Other rows contain satellites of the primary modulation. The separation of the satellites is twice the modulation vector, and, using the $y=0.2$ sample as an example, this distance corresponds in real space to $4.5b$. This yields a secondary modulation vector equivalent to $9.0b$, which is twice the $4.5b$ primary modulation (for $y=0.2$). Using the four-dimensional notation of de Wolff *et al.* for incommensurate superlattices, the satellites in Figs. 4(c) and 4(d) around the forbidden $\bar{1}00$ (or $\bar{1}000$) position would be $\bar{1}00\frac{1}{2}$ and $\bar{1}00\frac{\bar{1}}{2}$.

In contrast, only satellites for the primary modulation were observed in samples with lower nominal Y contents: $y=0.0$, 0.075, 0.09, and 0.12. Again using the four-dimensional notation, these spots would be indexed as $\bar{1}001$ and $\bar{1}00\bar{1}$ for first-order satellites around $\bar{1}000$. We note that, even though the $\bar{1}000$ reflection is forbidden, it appeared very weakly in all strongly exposed [001] patterns for $y=0.0$, 0.075, 0.09, and 0.12. Its presence is almost certainly due to reciprocal-lattice rods from higher layers. Specifically, $\bar{1}010$ is an allowed reflection. With this in mind, it is significant that, in samples exhibiting the secondary modulation, $\bar{1}000$ was indeed truly absent, even in the most strongly exposed patterns.

Kulik *et al.*[22] found remarkably similar evidence of a secondary modulation in $Bi_2Sr_2Ca_{1-x}Gd_xCu_2O_8$, where $0.85<x<1.0$. In [010] zone-axis diffraction patterns they found $10l$ reflections to be absent for materials exhibiting the secondary modulation. If this were also the case for our Y-substituted material exhibiting the secondary modulation, then intensities at the $\bar{1}00$ position derived from higher layers (e.g., $\bar{1}01$) would not be expected. So, the lack of forbidden $\bar{1}00$ spots in the secondarily modulated samples and their presence in normal $Bi_2Sr_2Ca_1Cu_2O_8$ samples are consistent with structural differences found elsewhere in [100] and [010] zone-axis diffraction patterns.

Highly specific streaking was observed in SAED patterns for compositions $y=0.2$, 0.5, and 1.0. For the $y=0.2$ sample, some heterogeneity between crystals was observed. In one sample, diffuse streaking along the b^* direction was found between (i.e., connecting) first-order satellites for the secondary modulation (e.g., between $\bar{1}00\frac{1}{2}$ and $\bar{1}00\frac{\bar{1}}{2}$). In a second foil [Fig. 4(c)], the streaking was restricted between first- and second-order satellites of the secondary modulation ($\bar{1}00\frac{1}{2}$ and $\bar{1}00\frac{3}{2}$). In both cases images revealed apparent stacking disorder along b and the streaking is presumably associated with this. In the pure Y sample [$y=1.0$; Fig. 4(d)], very weak streaking was observed between first- and second-order satellites for the secondary modulation (e.g., between $100\frac{1}{2}$ and $100\frac{\bar{1}}{2}$), as in the case of one foil of $y=0.2$.

In the $y=0.5$ sample, the electron-diffraction evidence may suggest incipient development of the secondary modulation. Streaking occurs along the b^* direction through 1001 and $100\bar{1}$ satellites, but not through 1000 spots, which as noted above occur from higher layers. These streaks, however, show a weak maximum at the position of the secondary satellites, possibly suggesting a poor development of a secondary modulation.

We want to emphasize that the electron-diffraction studies were performed on large, thin single crystals, and therefore we were able to correlate the structure with the composition and the electronic transport properties quite accurately. In some cases we measured electrical resistivity on the very same crystal used in the electron microscopy. As discussed later in greater detail, superconductivity disappears at about [Y]=0.45. Remarkably, the secondary modulation appears at about the same Y concentration. It remains to be seen if this is a simple coincidence or if there is a fundamental relationship between these subtle structural features and the conduction electrons in the material.

ELECTRONIC TRANSPORT

A primary motivation for replacing calcium with yttrium in these oxide superconductors was to change the carrier concentration, and to observe how this affected transport properties of the metal. In introducing Y^{3+} for Cu^{2+}, one would expect a decrease in the number of holes since it is well known that, in $Bi_2Sr_2CaCu_2O_8$, the dominant charge carriers are hole type. This has been demonstrated by the positive Hall coefficient measured for all temperatures.[1-3,6,25,27-29]

We have studied the dc electrical resistivity and Hall coefficient of the Y-doped samples described above. Results of optical transmission[10,11] and tunneling[12] studies on the undoped samples, as well as resistivity[30,31] and Hall[25,31] data for selected metallic and insulating specimens have been reported earlier.

For resistivity and Hall-effect measurements, very thin, regularly shaped single crystals were prepared. Typical dimensions were 1 mm$\times$0.5 mm$\times$1 μm for superconducting samples and 1 mm$\times$0.5 mm$\times$(1–10) μm for semiconductors, the smallest dimension being along the crystallographic c axis. Electrical contacts were made using 12-μm-diam gold wires and silver epoxy fired at 600 °C. Contact resistances were typically less then 1Ω. The a-b plane resistivity was measured using line contacts in a conventional four-probe arrangement.

For the Hall effect, two line contacts (for current) and three point contacts (for voltage) were attached. The voltage probes were arranged so that the ohmic voltage and the Hall voltage could be measured independently. A 70-kG magnetic field was applied parallel to the c axis. At a given temperature and current, the samples were repeatedly rotated in the magnetic field by 180° and voltage readings were taken. This method allowed us to separate the ohmic and Hall contributions to the measured voltages. The Hall signal proved to be linear for currents up to 10 mA and magnetic fields up to 80 kG, the maximum values applied.

The temperature dependence of the Hall effect is especially interesting, particularly for the superconducting samples, and was discussed by us and others elsewhere.[2,25,29] In the present study, however, we concen-

TABLE II. The Hall coefficient and associated carrier density for different yttrium concentrations. All values presented were measured at 300 K. Eight coppers per formula unit is assumed.

Nominal	Measured	R_H(300 K) (cm^3/C)	Carrier density n (300 K) (#/cm^3)	Hole/Cu site
$Y=0$	$y=0$	1.8×10^{-3}	3.5×10^{21}	0.38
$Y=0.09$	$Y=0.30$	4.8×10^{-3}	1.3×10^{21}	0.14
$Y=0.12$	$Y=0.44$	9.1×10^{-3}	6.9×10^{20}	0.07
$Y=0.20$	$Y=0.55$	1.8×10^{-2}	3.5×10^{20}	0.038
$Y=1.0$	$Y=0.86$	1.0	6.4×10^{18}	0.000 68

trate on the reasonably temperature-independent 300-K values, which, in turn, depend strongly on the Y concentration. For the purposes of comparison we apply the formula

$$R_H = 1/nec \tag{1}$$

to convert the Hall coefficient R_H to carrier density n.

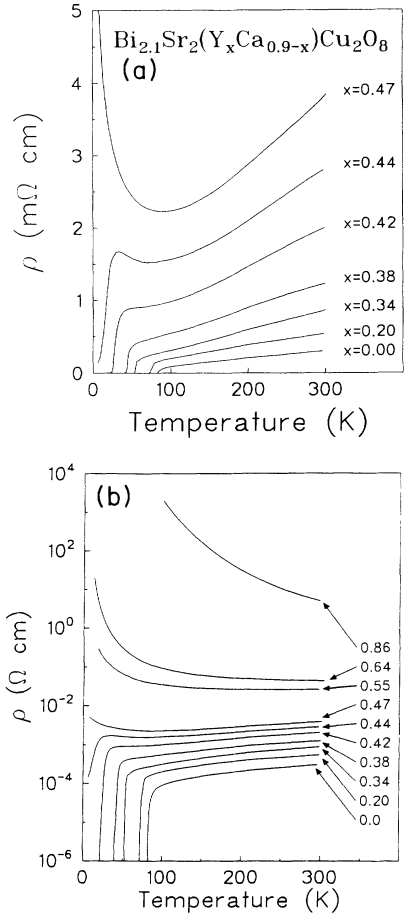

FIG. 5. Resistivity is plotted as a function of temperature for various single crystals in the family $Bi_2Sr_2Ca_{1-y}Y_yCu_2O_8$. (a) displays the metallic samples on a linear resistivity scale, while (b) uses a logarithmic resistivity scale to include the insulating specimens. The addition of yttrium gradually reduces the superconducting transition temperature to zero. For yttrium contents above $y=0.45$, the crystals become semimetallic and eventually insulating.

Table II gives the room-temperature (300 K) Hall coefficient, hole carrier density, and [hole]/[Cu] for different members of the study. These results substantiate the assumption that substituting Y for Ca subtracts from the hole concentration, thereby increasing the Hall voltage.

Figure 5 shows resistivity data for the various members of the Y-doping study. We plotted the results with both linear and logarithmic vertical scales so that the metals and insulators can all be viewed. For low Y concentrations, an increase in resistivity and a decrease in T_c are the most obvious results of the doping study. At high Y concentrations, there is a metal-insulator transition which takes place near a measured Y content of 0.45.

As an independent determination of T_c and superconducting transition width, a measurement of the diamagnetic shielding has been performed on several members of the study. This is an ac measurement which involves a colinear inductance pair separated by a distance of roughly 3 mm. A cleaved sample is placed between the pair with its c axis parallel to the line. An ac voltage is applied to one set of coils (the sender) and read across the other (receiver). The diamagnetic signature of the superconducting state manifests itself as a decreased signal at the receiver, due to the exclusion of the field from the

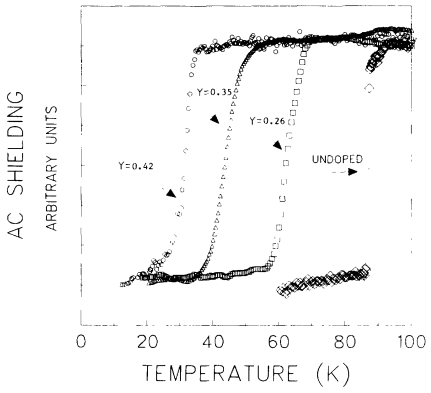

FIG. 6. ac magnetic shielding is plotted as a function of temperature for four different samples in the family $Bi_2Sr_2Ca_{1-y}Y_yCu_2O_8$, with the yttrium concentrations shown. The decrease in superconducting transition temperature with increased doping is evident. Although the units are arbitrary and the measurement yields no information about Meissner fraction, it reveals not only T_c but also transition width for very thin single crystals without making electrical contacts.

TABLE III. Properties of metallic members of the yttrium-doping study (a sample is arbitrarily defined as "metallic" if the resistivity vs temperature has a positive slope around room temperature). Data with an asterisk are interpolated from other measurements. Resistivity is interpreted using Matthiessen's rule: $\rho = m^*/ne^2\tau + m^*a/ne^2T$ as discussed in the text.

Nominal	Actual	n (cm^{-3})	ρ_0 ($\mu\Omega$ cm)	$d\rho/dT$ (300 K) ($\mu\Omega$ cm)/K	m^*/τ (g/sec)	m^*a (g/K sec)	$1/a\tau$ (K)
$Y=0$	$Y=0$	3.5×10^{21}	0	1.0	0	8.9	0
$Y=0.06$	$Y=0.20$	2.1×10^{21}*	0.25	2.1	700	9.1	76
$Y=0.075$	$Y=0.25$	1.7×10^{21}*	0.40	3.0	1090	9.1	110
$Y=0.09$	$Y=0.30$	1.3×10^{21}	0.80	4.0	1100	8.3	130

sample volume. This technique is more sensitive to secondary phases within a sample than is resistivity, which may be shorted out by a single superconducting filament.

Figure 6 shows normalized shielding signals from superconducting members of the Y-doping study. The corroboration of both T_c and transition sharpness seen in the resistivity measurements is evident from the figure. It should be stressed, however, that these were *not* the same crystals used for those measurements, and that these were not necessarily thin enough to call single crystals. Thus, the transitions may tend to be a bit wider and may occur at different absolute temperatures when compared with those from Fig. 5. Furthermore, the signal scale is arbitrary and is not meant to indicate Meissner fraction.

The narrow superconducting transition widths ($\simeq 2-3$ K) are indicative of high sample quality and homogeneity within a given crystal. The T_c for zero resistance in the calcium end member was $\simeq 88$ K and gradually declined to below 4.2 K (unmeasured) for the last metallic sample.

Another consequence of increased doping is the dramatic rise in extrapolated zero-temperature resistivity, ρ_0 (residual resistivity) presented in Fig. 7(b). The additional data points were measured in the same way as those appearing in Fig. 5. The scatter in the data is almost entirely due to sample variations within the same batch (especially in the Y-doped crystals) as well as to the relatively large error bar on the thickness measurement. This quantity (ρ_0) is zero for the calcium end member, but gradually increases before diverging in the insulating phase.

For metallic samples the interpretation of the residual resistivity data centers around Matthiessen's rule for scattering due to impurities and phonons.[30] Up to Y contents of $\simeq 0.4$, the data fit rather well (above the onset of superconductivity) with the empirical formula:

$$\rho = \rho_0 + \rho_{\rm ph}(T) , \tag{2}$$

where $\rho_0 = m^*/ne^2\tau$ and $\rho_{\rm ph} = m^*/ne^2\tau'$. The relaxation time for inelastic scattering (ordinarily the hole-phonon relaxation time), is assumed to be independent of the Y content and inversely proportional to T, i.e., $\tau' = 1/aT$. Within this approach the increase in residual resistivity observed in Figs. 5 and 7(b) is indicative of a rise in m^* and/or decreases in either carrier density or relaxation time. Since it has already been observed that carrier density decreases with increased doping, the only factor which remains to be calculated is the ratio of effective mass to relaxation time. Because ρ_0 is zero in the undoped case, it is clear that some impurity scattering has been brought on by the introduction of Y atoms into the lattice, this disorder being evident in the electron-diffraction data presented in Figs. 4(a)–4(d).

Table III presents the quantity m^*/τ as a function of yttrium content for those members of the study which display metallic (positive slope) resistivity at 300 K, and for which the carrier density is known from Hall-effect measurements. It should be stressed that, due to the temperature dependence of the Hall effect below 200 K for these samples, these values only bear upon high-temperature transport properties.

Figure 7(c) depicts the increase of the resistivity *slope*,

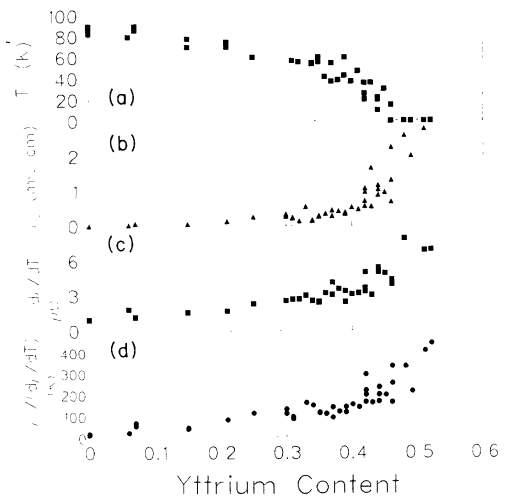

FIG. 7. Metallic and superconducting properties of the lightly doped single crystals are plotted as functions of measured yttrium content. (a) Superconducting critical temperature. (b) ρ_0 or "residual resistivity" defined as the zero-temperature intercept of the linear part of the resistivity curve, taken from measurements similar to those plotted in Fig. 5(a). (c) $d\rho/dT$ or slope of the resistivity vs temperature curves similar to those in Fig. 5(a). The slope is measured in the region of 300 K and so is positive even for a semimetallic sample. The 300 K slopes do become negative in the most highly doped samples, as is evident in Fig. 5(b). (d) $\rho_0/(d\rho/dT)$. The residual resistivity divided by the resistivity slope, both numbers coming from the data plotted in (b) and (c). In terms of a Matthiessen's rule interpretation, this quantity plots the ratio of a/τ, the ratio of the "strength" of the inelastic relaxation "a" to the relaxation time "τ."

$d\rho/dT$, with increased doping up to the metal-insulator transition. From Eq. (2) (semiclassical dc model), one would expect that

$$d\rho/dT = m^* a/ne^2 , \quad (3)$$

where a is the "strength" of the inelastic relaxation in the expression $1/\tau' = aT$. The graph in Fig. 7(c), then, shows the doping dependence of the quantity $m^* a/n$. Repeating the analysis performed on ρ_0 isolates the quantity $m^* a$ for those samples for which carrier density is available, as given in Table III.

Figure 7(d) shows the yttrium concentration dependence of the quantity $\rho_0/(d\rho/dT) = 1/a\tau$. The striking feature of this data is an apparent discontinuity for dopant values near the metal-insulator transition ($y \simeq 0.45$). It would appear that, on the lower side of the transition, there is a linear increase consistent with Matthiessen's rule approach, which assumes a metal with both impurity and phonon scattering. In the *insulating* phase, however, this model breaks down and another explanation must be sought. It has been argued[31] that the divergence of the resistivity at low temperatures, combined with the invariance of the Hall coefficient ($1/nec$), indicates a localization of the charge carriers.

CONCLUSIONS

We have succeeded in growing, preparing, and measuring the properties of high-quality single crystals in the family $Bi_2Sr_2Ca_{1-y}Y_yCu_2O_8$. In corroboration of the earlier studies,[1-9,22,21,23,24] we found that the principal characteristics of the structure do not change. The c-axis lattice spacing follows a linear relationship with the Y content. All samples have a superlattice, breaking the tetragonal symmetry in the ab plane. We describe subtle changes in the superlattice structure as the Y content varies; in particular, we observe a decline in the long-range order (as evidenced by broader Bragg spot sizes, and the fact that the crystals are smaller) with increases in Y-doping concentration. X-ray fluorescence analysis has yielded a slightly off-stoichiometric composition and the tendency to preferentially incorporate Y into the Ca lattice sites. Sample quality has been verified using electron microprobe analysis, as well as superconducting transition width.

Electrical transport measurements indicate a decrease in hole carrier density and concomitant increase in resistivity with heavier doping. Around [Y]=0.45, the ground state of the system exhibits a metal-insulator transition. We presented a detailed analysis of this transition earlier.[31] Apparently, there is no metallic ground state; at $T=0$ the material is either superconductor or insulator, which is a property of the two-dimensional electron gas.[31] The doping of 2:2:1:2 with yttrium has yielded a series of high-quality single-crystal samples with a variety of T_c and clearly illustrates the possibility of tuning both normal-state and superconducting properties of the solid with a change in only one starting (oxygen was not measured) compositional component.

In this work we summarize our results on the structural and electronic transport properties of $Bi_2Sr_2Ca_{1-y}Y_yCu_2O_8$. Some of the samples described here were selected for further study, including infrared transmission[10,11] and break-junction tunneling[12] measurements. The comprehensive study of these compounds, performed on single-crystal samples, yields insight not only into high-temperature superconductivity, but also into weak localization and metal-insulator transitions.

ACKNOWLEDGMENT

This work has been supported by NSF Grant No. DMR 9016456.

*Permanent address: Institute of Physics of the University, 41001 Zagreb, Croatia.

†Present address: Department of Geological Sciences, University of Kentucky, Lexington, KY 40506-0059.

[1]D. B. Mitzi, L. W. Lombardo, A. Kapitulnik, S. S. Laderman, and R. D. Jacowitz, Phys. Rev. B **41**, 6564 (1990).

[2]T. Tamegai, K. Koga, K. Suzuki, M. Ichihara, F. Sakai, and Y. Iye, Jpn. J. Appl. Phys. **28**, L112 (1989).

[3]A. Maeda, M. Hase, I. Tsykada, K. Noda, S. Takebayashi, and K. Uchinokura, Phys. Rev. B **41**, 6418 (1990).

[4]R. Yoshizaki, Y. Saito, Y. Abe, and H. Ikeda, Physica C **152**, 408 (1988).

[5]Noburu Fukushima, Hiromi Niu, and Ken Ando, Jpn. J. Appl. Phys. **27**, L1432 (1988).

[6]Ando, K. Fukuda, S. Kondoh, M. Sera, M. Onoda, and M. Sato, Solid State Commun. **67**, 815 (1988).

[7]A. Manthiriam and J. B. Goodenough, Appl. Phys. Lett. **53**, 420 (1988).

[8]W. A. Groen, D. M. DeLeeuw, and L. F. Feiner, Physica C **165**, 55 (1990).

[9]P. Mandal, A. Poddar, B. Ghosh, and P. Choudhury, Phys. Rev. B **43**, 13 102 (1991).

[10]D. B. Romero, G. L. Carr, D. B. Tanner, L. Forro, D. Mandrus, L. Mihaly, and G. P. Williams, Phys. Rev. B **44**, 2818 (1991).

[11]L. Forro, G. L. Carr, G. P. Williams, D. Mandrus, and L. Mihaly, Phys. Rev. Lett. **65**, 1941 (1990).

[12]D. Mandrus, L. Forro, D. Koller, and L. Mihaly, Nature **351**, 460 (1991).

[13]L. Forro, D. Mandrus, R. Reeder, B. Keszei, and L. Mihaly, J. Appl. Phys. **68**, 4876 (1990).

[14]L. Forro, J. R. Cooper, B. Leonitic, and B. Keszei, Europhys. Lett. **10**, 371 (1989).

[15]M. F. Crommie, Amy Y. Liu, Marvin L. Cohen, and A. Zettl, Phys. Rev. B **41**, 2525 (1990).

[16]The program, written at the Naval Research Laboratories, and in constant use, relies on user-fed information, most heavily on the product of the nominal sample density and thickness (g/cm^2). Performing this analysis on the calibration samples revealed the need for correction factors for certain peaks. The program was originally designed for use on K spectral lines; we found that we can use if for the Bi L with a relatively large (1.70) correction factor. Some elements were analyzed from two separate peaks, with good agreement between the two results.

[17]B. Batlogg, T. T. M. Palstra, L. F. Schneemeyer, R. B. Van

Dover, and R. J. Cava, Physica C **153-155**, 1062 (1988).
[18]Anthony K. Cheetham and Ann M. Chippendale (unpublished).
[19]W. Urland and F. Tietz, Solid State Commun. **69**, 995 (1989).
[20]S. Martin, A. T. Fiory, R. M. Flemming, L. F. Schneemeyer, and J. V. Waszczak, Phys. Rev. Lett. **23**, 2194 (1988).
[21]T. Onozuka, Y. Iwabuchi, T. Fukase, H. Sato, and T. E. Mitchell, Phys. Rev. B **43**, 13 066 (1991).
[22]J. Kulik, Y. Y. Xue, Y. Y. Sun, and M. Bonvalont, J. Mater. Res. **5**, 1625 (1990).
[23]X. B. Kan, J. Kulik, P. C. Chow, S. C. Moss, Y. F. Yan, J. H. Wang, and Z. X. Zhao, J. Mater. Res. **5**, 731 (1990).
[24]M. J. Casanove, P. Baules, E. Snoeck, and C. Roucau, Physica C **159**, 461 (1989).
[25]L. Forro, D. Mandrus, C. Kendziora, L. Mihaly, and R. Reeder, Phys. Rev. B **42**, 8704 (1990).
[26]A. Ourmazd, J. A. Rentschler, J. C. H. Spence, M. O'Keefe, R. J. Graham, D. W. Johnson, Jr., and W. W. Rhodes, Nature **327**, 308 (1987).
[27]C. Kendziora, L. Forro, D. Mandrus, and L. Mihaly (unpublished).
[28]J. Clayhold, N. P. Ong, P. H. Hor, and C. W. Chu, Phys. Rev. B **38**, 7016 (1988).
[29]G. Briceno and A. Zettl, Phys. Rev. B **40**, 11 352 (1989).
[30]D. Mandrus, L. Forro, C. Kendziora, and L. Mihaly, Phys. Rev. B (to be published).
[31]D. Mandrus, L. Forro, C. Kendziora, and L. Mihaly, Phys. Rev. B **44**, 2418 (1991).

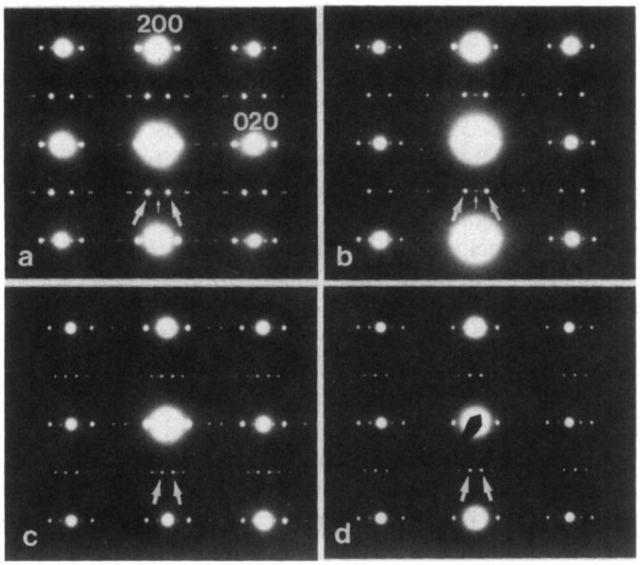

FIG. 4. [001] zone-axis selected-area electron-diffraction patterns of $Bi_2Sr_2Ca_{1-y}Y_yCu_2O_8$ thin specimens: (a) $y=0$, (b) $y=0.12$ nominal, (c) $y=0.2$ nominal, and (d) $y=1.0$ nominal. An incommensurate modulation occurs along the b^* direction, as indicated by the satellite reflections around, for example, 200 and 020. In (a) and (b), the corresponding first-order satellite reflections are indicated by arrows around the weak (and forbidden) $\bar{1}00$ spot (small arrow). In (c) and (d), first-order satellite reflections (arrows) are seen to have a separation half that in (a) and (b), and correspond to an apparent secondary modulation. In addition, the forbidden $\bar{1}00$ spot is absent in (c) and (d). In (c), diffuse streaking is observed between first- and second-order satellite reflections